CrossMark

Energy estimation and modeling solid thermal explosion containment on reactor for three organic peroxides by calorimetric technique

Yang-Fan Cheng[1,2] · Shang-Hao Liu[1,2] · Chi-Min Shu[1,2,3] · Bin Zhang[4] ·
Yun-Fei Li[4]

Abstract In this paper, we describe thermokinetic properties and decomposition characteristics of benzoyl peroxide, dicumyl peroxide, and lauroyl peroxide, which are widely used in the polymerization process as energy boosters. In the past, many accidents occurred that involved overpressure and runaway excursion of the process and thermal explosion. One reason for accidents is because of the peroxy group (–O–O–) of organic peroxides (OPs) due to its thermal instability and high sensitivity when exposing to heat. Apparent activation energy and pre-exponential factor were obtained during decomposition via non-isothermal well-recognized kinetic equation, fitting curve tests, and approximate solution to design safer reaction conditions when OPs are used as fuel. Moreover, the storage conditions were investigated for the simulation of thermal explosion in a 24-kg cubic box package and a 400-kg barrel reactor for commercial application. Experimental results established the novel features of solid explosion hazard of OPs.

List of symbols

A	Pre-exponential factor (s^{-1})
CT	Control temperature (°C)
C_p	Specific heat capacity (J g^{-1} °C^{-1})
E_a	Apparent activation energy (kJ mol^{-1})
ET	Emergency temperature (°C)
i	Component number
k_0	Pre-exponential factor
k_1, k_2	Rate constants of a reaction or stage
NC	Number of components
n	Unit outer normal on the boundary
n_1, n_2	Reaction orders of a specific stage
q	Heat flow rate (W)
R	Gas constant (J mol^{-1} K^{-1})
r	Reaction rate constant (mol l^{-1} s^{-1})
SADT	Self-accelerating decomposition temperature (°C)
T	Temperature of sample (K)
TCL	Time to conversion limit (day)
T_{cr}	Critical temperature (°C)
T_0	Exothermic onset temperature (°C)
T_f	Final temperature (K)
T_p	Peak temperature (°C)
t	Time (min)
TMR_{iso}	Time to maximum rate under isothermal conditions (day)
W	Heat power (J s^{-1})
z	Autocatalytic constant

✉ Shang-Hao Liu
shliu998@163.com

1 Department of Ammunition Engineering and Explosion Technology, Anhui University of Science and Technology (AUST), 168 Taifeng Street, Huainan 232001, Anhui, China

2 Research Center for Explosion Safety and Firework Material, AUST, 168 Taifeng Street, Huainan 232001, Anhui, China

3 Department of Safety, Health, and Environmental Engineering, National Yunlin University of Science and Technology, Douliou 64001, Taiwan, ROC

4 School of Chemical Engineering, AUST, 168 Taifeng Street, Huainan 232001, Anhui, China

ΔH_d	Heat of decomposition (J g^{-1})
α	Degree of conversion of a component
β	Scanning rate (°C min^{-1})
ρ	Density (kg m^{-3})

Introduction

Since the chemical accidents are frequently caused by runaway reaction, the importance issue of primary safety production provided by technology or research has emphasized that are intended to establish a more sustainable safety circumstance [1–3]. To solve this problem, our studies encompassed evaluating the thermokinetics of three organic peroxides (OPs) which existed in petrochemical industries inside the high-temperature reactors as well as complex thermodynamics of all the involved phases (solid, gas, and liquid).

Organic peroxides are extensively used as fuel, polymerization initiator, and cross-linking agent to offer tremendous energy in order to polymerize or oxidize the reaction system in complex chemicals systems [4–6]. As Fig. 1 illustrates, even if the purpose of mixing is to enhance performance, emerging energy hazards may be potentially created under unexpected conditions. Therefore, proper accident scenarios and thermal risk assessment models are needed to make use of OPs more safe and efficient [7–10].

However, numerous thermal explosions and runaway accidents have been caused by OPs due to unstable nature of O–O bond. For instance, *tert*-butyl hydroperoxide 70 mass % (−1622.4 J g^{-1}), *tert*-butyl peroxybenzoate 98 mass% (−1150.0 J g^{-1}), and cumene hydroperoxide 80 mass% (−1152.7 J g^{-1}) [4–12], which are essentially unstable and active, as given in Table 1 [12–14]. According to the previous database of OPs in many accidents, thermokinetic evaluation is one of the main methods to keep balance between high fuel productivity and inherently safer process design in the industry [15].

We performed a precise way to conduct thermal analysis of benzoyl peroxide (BPO), dicumyl peroxide (DCPO), and lauroyl peroxide (LPO), three typical OPs (Fig. 2), using differential scanning calorimetry (DSC) technique. In these examinations, we applied well-recognized kinetic equation, thermal safety software (TSS), and approximate solution at the scanning rates (β) of 0.5, 1, 2, and 4 °C min^{-1} for kinetic studies. Moreover, to observe the behaviors of decomposition and safer reaction conditions, the apparent activation energy (E_a) and pre-exponential factor (A) were obtained through applying Ozawa kinetic equation and approximate solution [16–18]. This was accomplished along with a comparison of the mathematical approaches to build up the thermal decomposition properties for these three solid OPs. With considerations of a number of petrochemical disasters occurred based on runaway reactions, it is the core focus of this article to measure the thermal safety parameters made over the past cases via innovations in the hybrid graphs.

On the other hands, the safer statement of commercial package and process reactor is also an important issue around the world. A 24-kg cubic box package and a 400-kg of barrel reactor via robust computational model were simulated to improve safety conditions [19]. The goals of this evaluation were to observe thermal decomposition of BPO, DCPO, and LPO with DSC technique and then to obtain the applicable parameters that will be used via nth-order and autocatalytic reaction models to assess thermal explosion hazard via simulation to predict the best energy effect and storage conditions.

This novel approach was to develop a green, precise, and cost-effective procedure for reduction in energy in thermal decomposition and explosion properties, such as heat of decomposition (ΔH_d), apparent activation energy (E_a), isothermal time to maximum rate (TMR$_{iso}$), pre-exponential factor (k_0), total energy release (TER), time to conversion limit (TCL), self-accelerating decomposition temperature (SADT), control temperature (CT), emergency temperature (ET), and critical temperature (T_{cr}) [20–22]. Therefore, the approaches could establish an effective technology for energy reduction in terms of thermal decomposition properties that includes the experiment and simulation for BPO, DCPO, and LPO [22–24].
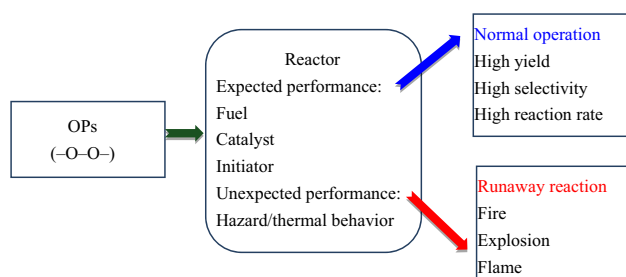
Materials and methods

Samples

LPO of 95 mass% in a solid powder form was purchased from Fluka. BPO of 75 mass% and DCPO of 98 mass% as two white crystalline solid substances were purchased from PRS Panreac and Aldrich, respectively. To alleviate any sensible heat release, they were stored in a refrigerator at 4 °C. Experimental techniques and equipments, such as

Fig. 1 A conceptual diagram of OPs with expected/unexpected effects

Table 1 Selected thermal explosion incidents occurred by peroxides [12–14]

Date	Chemical	Location	Injuries	Fatalities	Hazard	Cause
1964.07.14	MEKPO[a]	Japan	114	19	Explosion (storage)	External fire
1979.07.13	MEKPO	Taiwan	49	33	Explosion (storage)	Thermal decomposition
1981.04.21	CHP	Taiwan	3	1	Explosion (distillator)	Thermal decomposition
1982.02.18	MEKPO	Taiwan	55	5	Explosion (reactor)	Thermal decomposition
1986.05.02	CHP	Taiwan	0	0	Explosion (reactor)	Thermal decomposition
1987.09.15	H_2O_2[b]	Taiwan	20	0	Explosion (tank)	Incompatible contamination
1988.07.25	TBHP[c]	Taiwan	19	0	Explosion and fire (tank)	Cooling failure
1996.10.07	MEKPO	Taiwan	47	10	Explosion (tank)	Fire
1999.03.24	DCPO	Taiwan	0	0	Explosion	
2000.08.24	MEKPO	Korea	11	3	Explosion (storage)	Unknown
2003.01.02	BPO	USA	1	0	Explosion (dryer)	Thermal decomposition
2003.09.26	CHP/DCPO	Taiwan	2	0	Explosion	
2005.08.02	DCPO	Taiwan	0	0	Explosion	
2008.01.16	DCPO	Taiwan	0	0	Explosion (reactor)	Thermal decomposition
2009.06.22	TBHP	Taiwan	0	0	Explosion (reactor)	Thermal decomposition
2010.01.08	CHP	Taiwan	0	0	Explosion (reactor)	Catch fire
2011.07.26	H_2O_2	Taiwan	0	0		Fire (pipeline gas leak)

[a]Methyl ethyl ketone peroxide

[b]Hydrogen peroxide

[c]*tert*-butyl hydroperoxide

preliminary estimate, DSC, and reaction kinetic models, were explained in detail elsewhere [25].

Differential scanning calorimetry

Dynamic thermal scanning experiments were performed on a Mettler TA8000 system linked to a DSC 821[e] measurement test crucible (Mettler ME-26732), which is the essential part of the experimental evaluation. It was used for carrying out the experiments for withstanding relatively high pressure to approximately 100 bar. The ASTM E698 standard method was followed to obtain thermal curves for calculation of the kinetic parameters. STAR[e] software was used to obtain thermal curves for analysis [26–28]. In the final optimized procedure, the energy profile followed the four steps:

1. Scanning rate setup: scanning rate chosen for the temperature-programmed ramps were 0.5, 1, 2, and 4 °C min^{-1}.
2. Scanning range setup: range of temperature rise was selected from 30 to 300 °C.
3. Sample mass setup: about 5 mg of the samples was used for acquiring the experimental data.
4. Test cell composition setup: test cell was sealed manually using a special tool equipped with Mettler's DSC instrument.

Reaction kinetic model simulations

The experimental data were processed, and the kinetics were evaluated using TSS program developed by ChemInform Saint-Petersburg (CISP) Ltd. A wide variety of thermal analysis systems have been used to investigate the chemical reactions kinetics [29]. The methods for development of kinetic model and algorithms that we used were clearly described elsewhere [30, 31]. In particular, TSS program demonstrates that numerical optimization methods are required to estimate parameters, such as E_a, A, TMR_{iso}, and TCL.

Solid thermal explosion simulations

After January 01, 2005, the Federal Motor Carrier Safety Administration (FMCSA) requires motor carriers to obtain a Hazardous Materials Safety Permit (HMSP) prior to transportation of certain highly hazardous materials [19]. In accordance with the above description, we used a 400-kg barrel reactor and a 25-kg cubic box as process reactor and commercial package, respectively, to simulate the thermal hazard of BPO, DCPO, and LPO. The radius, height, and shell thickness and the reactors boundary conditions are presented in Table 2 [29–31].
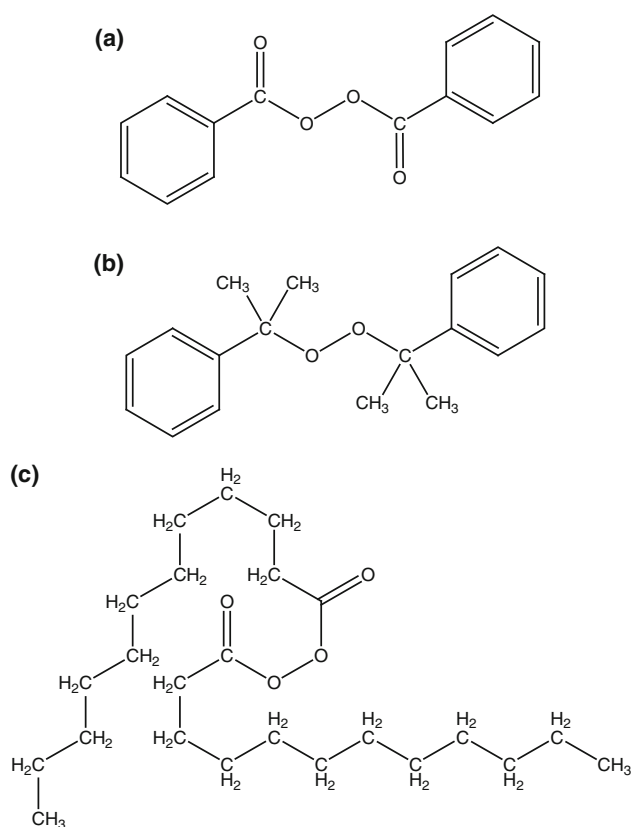
Fig. 2 The structure of three solid Ops. **a** BPO, **b** DCPO, **c** LPO [25, 27, 28]

Reaction kinetic model

The kinetic simulation model can represent complex multistage reactions that may consist of several independent, parallel, and consecutive stages, as illustrated in the following genres [30–32].

Simple single-stage reaction:

$$\frac{d\alpha}{dt} = k_0 e^{\frac{-E_a}{RT}} f(\alpha) \tag{1}$$

One-stage for nth-order reaction:

$$\frac{d\alpha}{dt} = k_0 e^{\frac{-E_a}{RT}} (1 - \alpha)^n \tag{2}$$

Multistage for autocatalytic reaction:

$$f(\alpha) = (1 - \alpha)^{n_1} (\alpha^{n_2} + z) \tag{3}$$

Reaction with two consecutive stages:

$$\frac{d\alpha}{dt} = k_1 e^{\frac{-E_1}{RT}} (1 - \alpha)^{n_1}; \quad \frac{d\gamma}{dt} = k_2 e^{\frac{-E_2}{RT}} (\alpha - \gamma)^{n_2} \tag{4}$$

Two-parallel reactions with full autocatalysis:

$$\frac{d\alpha}{dt} = r_1(\alpha) + r_2(\alpha); \quad \begin{array}{l} r_1(\alpha) = k_1(T)(1 - \alpha)^{n_1} \\ r_2(\alpha) = k_2(T)\alpha^{n_2}(1 - \alpha)^{n_3} \end{array} . \tag{5}$$

Results and discussion

Non-isothermal analysis of DSC data

The heat flow curves versus temperature for the thermal decomposition of BPO, DCPO, and LPO examined with DSC technique are shown in Figs. 3–5. Thermal decomposition properties, such as apparent onset temperature (T_0), peak temperature (T_p), final temperature (T_f), and heat of reaction (ΔH_d), were acquired using STAR^e software. The collected data were used to evaluate the behaviors of thermal hazard and exothermic reaction, as summarized in Table 3.

In accordance with DSC examinations, T_0 can provide information about the reaction characteristics and rudimentary thermal hazards when OPs are decomposed under non-isothermal conditions. It is obvious that the characteristic features of DSC curve for each individual solid of this type is the absence of melting peak in the endothermic reaction. The exothermic curve has a brief period of changing from solid to liquid phase under physical transformation for solid OPs. The DSC thermal curves of solid OPs with quick-decomposition character (especially BPO) reveal exothermic decomposition reactions that take place in parallel with physical phase changes in narrow

Table 2 The reactor size and boundary conditions for the 25-kg cubic box and 400-kg barrel reactor by simulation

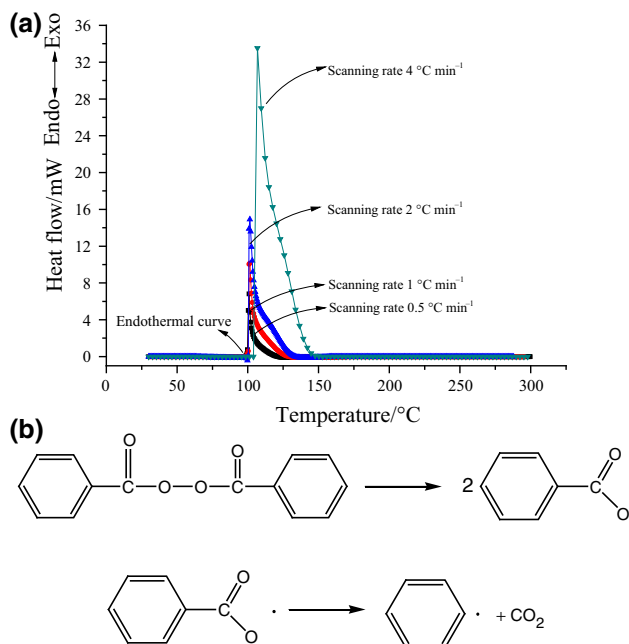| Package size/kg	Radius/m	Height/m	Shell thickness/m	Boundary conditions	X/W m^{-2} K^{-1}	Density/kg m^{-3}
25	0.20	0.30	0.015	Top/3rd kind	10/10/10	900
				Side/3rd kind		
				Bottom/3rd kind		
400	0.38	1.22	0.038	Top/3rd kind	10/10/10	900
				Side/3rd kind		
				Bottom/3rd kind		

Fig. 3 **a** DSC thermal curves of heat flow versus temperature for BPO decomposition with scanning rates of 0.5, 1, 2, and 4 °C min^{-1}, **b** the decomposition reaction mechanism of BPO [33]
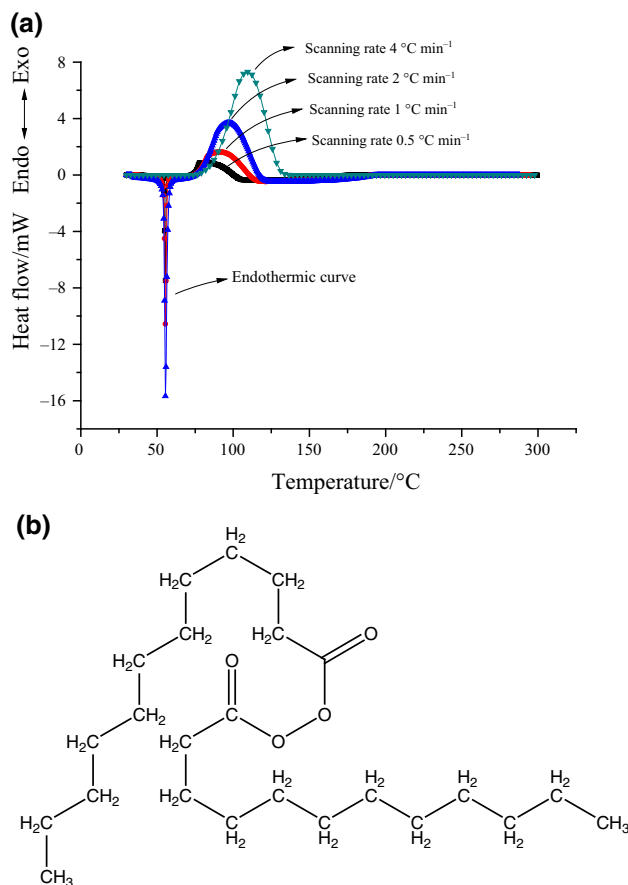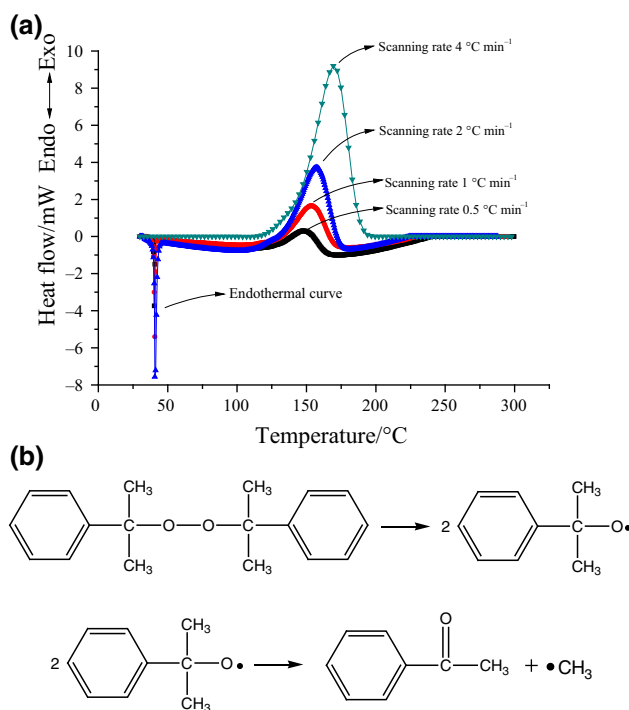

Fig. 4 **a** DSC thermal curves of heat flow versus temperature for DCPO decomposition with scanning rates of 0.5, 1, 2, and 4 °C min^{-1}, **b** the decomposition reaction mechanism of DCPO [35, 36]

Fig. 5 **a** DSC thermal curves of heat flow versus temperature for LPO decomposition with scanning rates of 0.5, 1, 2, and 4 °C min^{-1}, **b** the decomposition reaction mechanism of LPO [21]

Table 3 Results of experimental data for BPO, DCPO, and LPO's thermal decomposition via STAR^e software by DSC tests

Organic peroxide Substance	β/°C min^{-1}	Mass/mg	T_0/°C	T_p/°C	T_f/°C	ΔH_d/ J g^{-1}
BPO 75 mass%	0.5	5.0 ± 0.2	100	100	102	758
	1.0		101	102	105	875
	2.0		103	104	110	845
	4.0		104	107	119	1045
DCPO 98 mass%	0.5	5.0 ± 0.2	107	148	168	766
	1.0		130	155	178	733
	2.0		136	162	179	716
	4.0		142	170	187	911
LPO 97 mass%	0.5	5.0 ± 0.2	88	108	129	573
	1.0		77	93	95	654
	2.0		80	100	122	707
	4.0		88	109	129	573

temperature intervals of endothermic melting process, as shown in Fig. 3.

The faster scanning resulted in wider and smoother thermal curves and unstable conversion rate of thermal decomposition (Figs. 3–5). The exothermic decomposition reactions of solid OPs induce in the liquid phase were measured when the liquid and solid phases coexist. The enormous energy flow from the exothermically decomposing liquid is capitalized on the endothermic melting of the solid, so that the system is maintained under isothermal conditions until the melting is completed.

In particular, as the environmental temperature exceeds T_0, the exothermic peak of BPO was observed as sharper as and much more precipitous than those of DCPO and LPO. Table 3 displays the thermokinetic parameters for thermal decomposition phenomenon at non-isothermal conditions, indicating that the induction period will be too short to acquire the integral from free radical reaction under the heating condition from T_0 (100–104 °C) to T_P (100–107 °C) at 0.5, 1, 2, and 4 °C min^{-1} with huge energy generation from decomposition of oxygen–oxygen bond. Therefore, process engineers must exercise much care about energy generation and energy removal rate in a batch reactor system.

Non-isothermal kinetic method

Calculation of thermokinetic parameters using Ozawa kinetic equation

This method is applicable to the DSC integral-type thermal curves. Formal models can be expressed on the basis of scanning rate that may consist of several dependent equations, as illustrated in the following types [19–21]:

$$\ln(\beta) = -1.0516 \frac{E_a}{RT_P} + \text{const} \tag{6}$$

A set of kinetic equations can be derived at various scanning rates [19–21]:

$$\ln \beta_1 + 1.0516 \frac{E_a}{RT_{P_1}} = \ln \beta_2 + 1.0516 \frac{E_a}{RT_{P_2}}$$
$$= \ln \beta_3 + 1.0516 \frac{E_a}{RT_{P_3}} = \cdots \tag{7}$$

The activation energy analysis graphs for BPO, DCPO, and LPO at scanning rates of 0.5, 1, 2, and 4 °C min^{-1} using kinetic equation are illustrated in Figs. 6–8. From Tables 4–6, the E_a values, computed from the kinetic equation, are 130, 124, and 133 kJ mol^{-1}, and the correlation coefficients are 0.975, 0.991, and 0.983 for the three solid OPs of BPO, DCPO, and LPO, respectively.
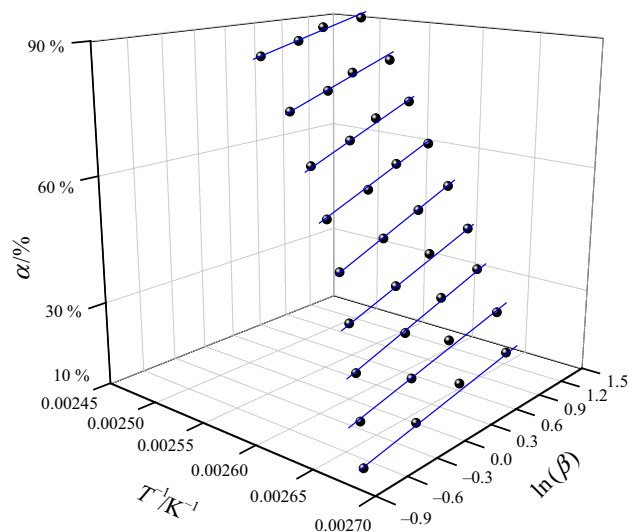

Fig. 6 Activation energy analysis graphs for BPO at scanning rates of 0.5, 1, 2, and 4 °C min^{-1} under α at 10, 20, 30, 40, 50, 60, 70, 80, and 90% by Ozawa–Flynn–Wall kinetic equation
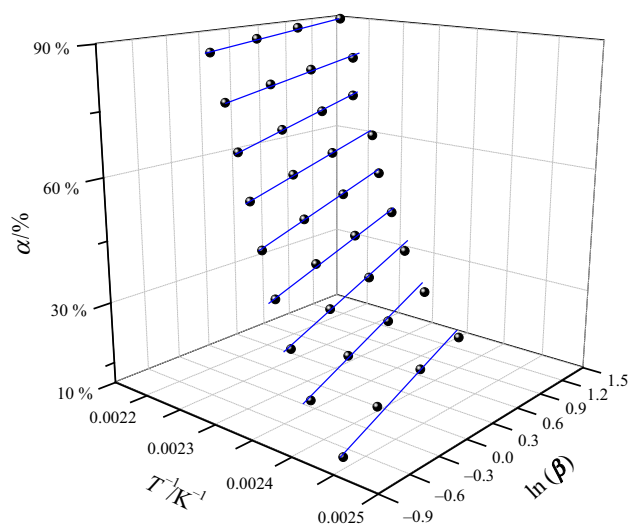

Fig. 7 Activation energy analysis graphs for DCPO at scanning rates of 0.5, 1, 2, and 4 °C min^{-1} under α at 10, 20, 30, 40, 50, 60, 70, 80, and 90% by Ozawa–Flynn–Wall kinetic equation

Determination of thermokinetic parameters using kinetic model simulation

The kinetic parameters were determined with TSS program from the DSC data, as listed in Table 7. According to a previous study, the thermal decomposition of BPO was considered as an autocatalytic reaction and that of DCPO and LPO as the nth-order reaction [14, 21, 36]. In addition, comparisons of experimental data and simulation results for: time to the maximum rate under isothermal condition
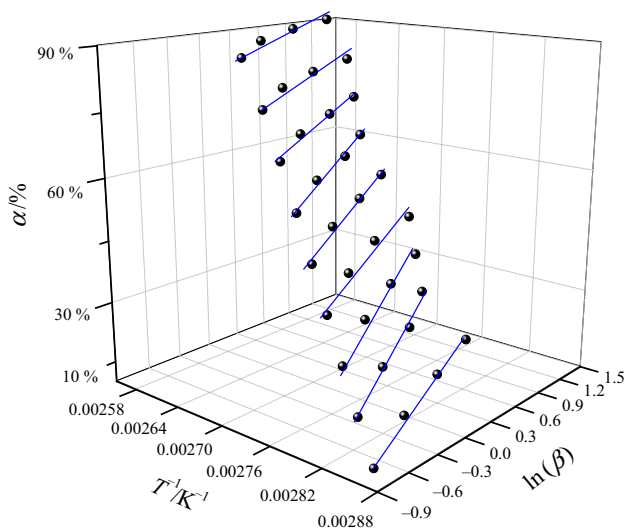
Fig. 8 Activation energy analysis graphs for LPO at scanning rates of 0.5, 1, 2, and 4 °C min^{-1} under α at 10, 20, 30, 40, 50, 60, 70, 80, and 90% by Ozawa–Flynn–Wall kinetic equation

Table 5 DCPO's thermokinetic parameters for the thermal decompositions in various degrees of conversion 10, 20, 30, 40, 50, 60, 70, 80, and 90% by Ozawa–Flynn–Wall kinetic equation

α/%	E_a/kJ mol^{-1}	Correlation coefficient/R^2	Standard deviation (SD)
10	150.6	0.994	0.057
20	140.2	0.984	0.045
30	138.6	0.996	0.033
40	133.2	0.986	0.065
50	119.2	0.991	0.064
60	120.5	0.994	0.061
70	110.1	0.976	0.068
80	103.1	0.981	0.071
90	105.5	0.989	0.034
Average	124.5		
Literatures	124.5[a], 135[b]		

[a]Lu et al. [35]

[b]Wu et al. [36]

Table 4 BPO's thermokinetic parameters for the thermal decompositions in various degrees of conversion 10, 20, 30, 40, 50, 60, 70, 80, and 90% by Ozawa–Flynn–Wall kinetic equation

α/%	E_a/kJ mol^{-1}	Correlation coefficient/R^2	Standard deviation (SD)
10	149.2	0.922	0.142
20	120.3	0.981	0.140
30	122.7	0.980	0.091
40	130.9	0.983	0.064
50	131.4	0.985	0.042
60	121.5	0.989	0.044
70	140.3	0.998	0.058
80	130.5	0.994	0.085
90	124.8	0.965	0.097
Average	130.1		
Literatures	131.2[a], 137.8[b]		

[a]Lu et al. [33]

[b]Zaman et al. [34]

Table 6 LPO's thermokinetic parameters for the thermal decompositions in various degrees of conversion 10, 20, 30, 40, 50, 60, 70, 80, and 90% by Ozawa–Flynn–Wall kinetic equation

α/%	E_a/kJ mol^{-1}	Correlation coefficient/R^2	Standard deviation (SD)
10	151.2	0.899	0.154
20	144.1	0.920	0.137
30	134.4	0.964	0.093
40	133.1	0.982	0.066
50	124.5	0.993	0.040
60	125.9	0.992	0.043
70	130.2	0.986	0.057
80	129.2	0.970	0.084
90	133.1	0.961	0.096
Average	133.9		
Literature	136.4[a]		

[a]Duh et al. [37]

(TMR$_{iso}$) and time until 10% conversion limit (TCL) for BPO, DCPO, and LPO were conducted and the observations are presented in Figs. 9–11, respectively. From the above kinetic model simulation, the values of E_a for BPO, DCPO, and LPO were computed as 130, 134, and 140 kJ mol^{-1}, respectively. Overall, the E_a values of 130, 124, and 133 kJ mol^{-1} are similar to the values obtained from Ozawa–Flynn–Wall kinetic equation and kinetic model simulation methods. It will be beneficial to corroborate the advantages of the model fitting via TSS program.

Moreover, the TMR$_{iso}$ and TCL values, indicating estimation of the parameters at the earliest stages of the life

Table 7 Thermokinetic parameters evaluated by simulation

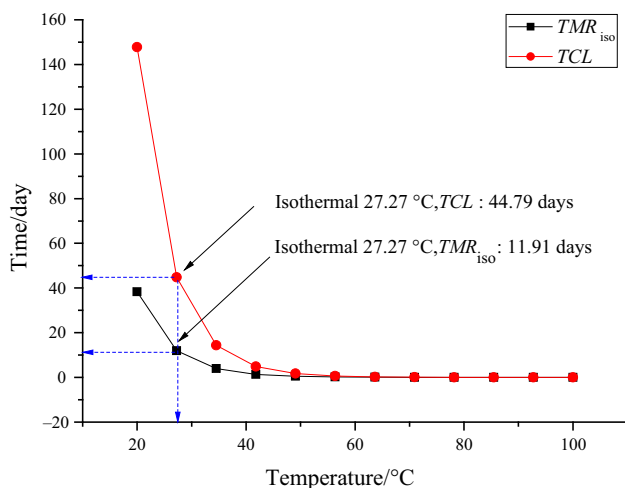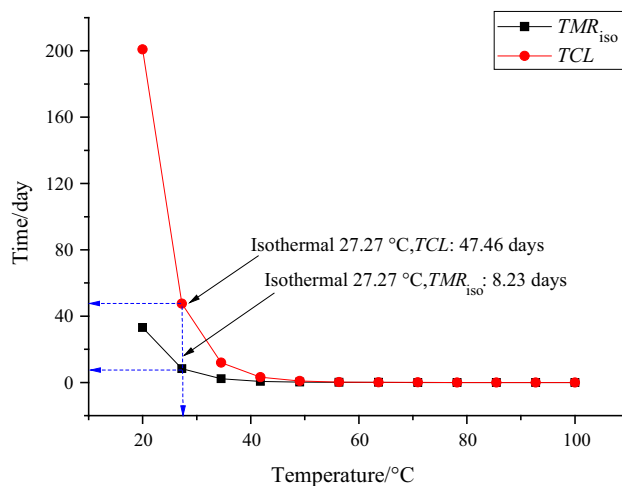| Substance	BPO	DCPO	LPO
Kinetic model	Autocatalytic	nth-order	nth-order
ln(k_0)/lns^{-1}	32.88	31.43	40.73
E_a/kJ mol^{-1}	130.16	134.90	140.27
Reaction order (n/nth)	N/A	0.94	1.38
Reaction order (n_1/auto)	1.6	N/A	N/A
Reaction order (n_2/auto)	0.6	N/A	N/A
Autocatalytic constant/z	3.00E−03	N/A	N/A
ΔH_d/kJ kg^{-1}	1494.99	907.99	575.13

Fig. 9 TMR_{iso} and TCL (10% conversion) of BPO achieved with autocatalytic kinetic simulation

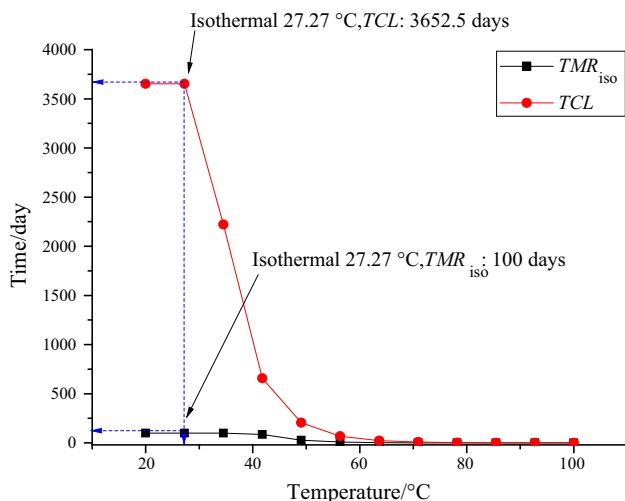**Fig. 11** TMR_{iso} and TCL (10% conversion) of LPO achieved with autocatalytic kinetic simulation

Evaluation of thermokinetic parameters via approximate solution

This section describes the development of the mathematical model of the nth-order system under dynamic experiment. Analytical expressions are also derived to be used in the whole reaction in the systems with both linear and Frank–Kamenetskii kinetic. The kinetic behavior of a wide range of an nth-order system can be well approximated through the prototype step:

$$-r_a = -\frac{dC_A}{dT} = k_0 e^{-\frac{E_a}{RT}} C_A^n \tag{8}$$

From the identification of decomposition, the conversion rate is expressed as Eq. (9) and the reactant concentration can be estimated using Eqs. (10) and (11):

$$\alpha = \frac{C_{A0} - C_A}{C_{A0}} \tag{9}$$

$$C_{A0}\alpha - C_{A0} = -C_A \tag{10}$$

$$C_A = C_{A0}(1 - \alpha) \tag{11}$$

Taking the differentiation on both sides of the equation results in:

$$-\frac{dC_A}{dt} = \frac{d\alpha}{dt} \tag{12}$$

Substitution of Eq. (8) into Eq. (12) and simplification of the equation gives Eq. (14):

$$\frac{d\alpha}{dt} = k_0 e^{-\frac{E_a}{RT}} C_{A_0}^n (1 - \alpha)^n \tag{13}$$

Fig. 10 TMR_{iso} and TCL (10% conversion) of DCPO achieved with autocatalytic kinetic simulation

cycle for the three OPs, were acquired via isothermal simulation, as displayed in Figs. 9–11. For further explanation, TMR_{iso} means the time of exothermic curve from beginning to maximum and TCL means the time of whole reaction when the reaction conversion was 10%. For example, Fig. 9 shows TMR_{iso} and TCL of BPO in which the values were simulated under various isothermal conditions. The storage temperature is less than 27.27 °C, which is beyond the upper limit of 11.94 and 44.79 days for TMR_{iso} and TCL separately.

$$\frac{d\alpha}{dt} = Ae^{-\frac{E_a}{RT}}f(\alpha) \tag{14}$$

The range of scanning temperature can be derived from Eqs. (15) and (16):

$$T - T_0 = \beta t \tag{15}$$

$$dT = \beta\, dt \tag{16}$$

Substitution of Eq. (16) into Eq. (14) and then integration results in Eq. (17) under Frank–Kamenetskii approximate solution [38, 39]:

$$\frac{d\alpha}{dT} = \frac{A}{\beta}e^{-\frac{E_a}{RT}}f(\alpha) \tag{17}$$

$$\int_0^\alpha \frac{d\alpha}{f(\alpha)} = \int_{T_0}^T \frac{A}{\beta}e^{-\frac{E_a}{RT}}dT \cong \left(\frac{A}{\beta}\right)\frac{RT^2}{E_a}e^{-\frac{E_a}{RT}} \tag{18}$$

To simplify the complex calculations, we consider $G(\alpha)$ as Eq. (19), and then Eq. (22) can be derived from Eqs. (19) to (21) via

$$G(\alpha) = \int_0^\alpha \frac{d\alpha}{f(\alpha)} \tag{19}$$

$$G(\alpha)f(\alpha) = \left(\frac{A}{\beta}\right)\frac{RT^2}{E_a}e^{-\frac{E_a}{RT}}f(\alpha) = \frac{RT^2}{E_a}\frac{d\alpha}{dt} \tag{20}$$

$$\frac{1}{G(\alpha)f(\alpha)} = \frac{E_a}{RT^2} \times \frac{dT}{d\alpha} \tag{21}$$

$$\int_0^\alpha \frac{d\alpha}{G(\alpha)f(\alpha)} = \int_0^T \frac{E_a}{RT^2}dT = -\frac{E_a}{R}\frac{1}{T} + const \tag{22}$$

Therefore, the E_a values of DCPO and LPO under the nth-order reaction assumption can be estimated using Eq. (22) with Frank–Kamenetskii approximate solutions. On the contrast, BPO was belonged to an autocatalytic reaction [14]. Figures 12 and 13 portray the regions of endothermic and exothermic characteristics of the patterns generated in the reaction process. The curves were divided into two parts on the y-axis that can be mathematically exactly determined. First of all, the value of y-axis briefly decreased, depending on the conversion rate, from 0.01 to 0.08 under endothermic reaction for physical change (Fig. 12). Then, it diminished steeply from 0.08 to 0.99 under exothermic reaction. The tendency was similar to DSC curve between Figs. 4 and 12. Finally, the E_a values computed via the approximate solution were obtained as 126 and 136 kJ mol^{-1} and the correlation coefficients were 0.987 and 0.988 for DCPO and LPO, respectively. This method identifies the further materials to estimate the E_a value applied in expected performance (fuel, catalyst, or initiator).

Generally, the complex procedure upon E_a for the OPs can be estimated using Eqs. (4), (7), and (22) together with
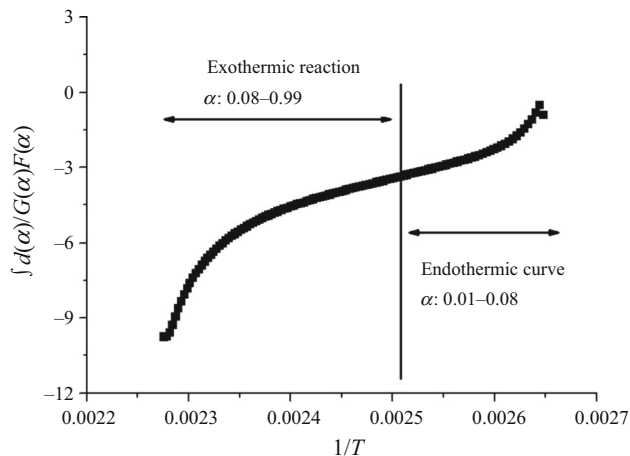

Fig. 12 Approximate solution of DCPO decomposition for apparent activation energy
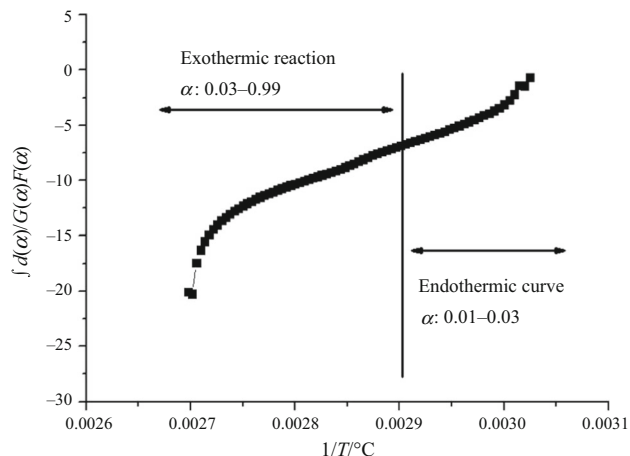

Fig. 13 Approximate solution of LPO decomposition for apparent activation energy

the equations for estimation of the solid-phase activity coefficient for the self-reactant component of the solution, as given in Table 8.

Barrel package and reactor thermal hazard simulations

Our goal was to develop a simple and swift green technology that could replace the inaccurate computations and complex tests through the traditional SADT tests. The chosen approach was to establish a procedure for thermal hazard assessment that included energy safety parameters [29–32], such as the SADT, CT, ET, and T_{cr}, for a container or reactor containing BPO, DCPO, or LPO.

In view of the application of safety, the energy hazard of solid OPs was simulated, the critical parameters for the

Table 8 Apparent activation energy of BPO, DCPO, and LPO determined by various methods

Substance	Ozawa–Flynn–Wall kinetic equation	Kinetic model simulation	Approximate solution	Reaction type
BPO	130	130	–	Autocatalytic
DCPO	124	134	126	nth-order
LPO	133	140	136	nth-order

Table 9 A comparison of the values from the literature and the solid thermal hazard simulation for the SADT, CT, ET, and TCR at DSC non-isothermal scanning rate of 0.5, 1, 2, and 4 °C min^{-1} in the 25-kg package and 400-kg reactor

Package/kg	Substance	SADT/°C from the literature	SADT/°C	CT/°C	ET/°C	T_{cr}/°C
25	BPO	68[a]	65	55	60	66
	DCPO	80[a], 77.8[b]	74	64	69	75
	LPO	50[a], 49[b]	46	36	41	47
400	BPO	N/A	61	51	56	62
	DCPO	N/A	70	60	65	71
	LPO	N/A	44	34	39	45

[a] Akzo Nobel [40]

[b] UN test [41]

energy hazard were numerically determined from the chemical kinetics for several types of reactor geometries and various boundary conditions, including the possibility of setting boundary shells and environmental situation. For solid energy hazard simulations, the following statements were applied from Eqs. (23) to (25) [29, 30, 39]:

Thermal conductivity equation:

$$\rho C_p \frac{\partial T}{\partial t} = \text{div}(\lambda \Delta T) + W \tag{23}$$

Kinetic equations (formal model):

$$\frac{\partial \alpha_i}{\partial t} = r \quad i = 1, \dots NC \tag{24}$$

Heat power equation:

$$W = \sum_{(i)} Q_i^{\infty} r_i \tag{25}$$

Initial fields of the temperature and conversions are supposed to be constant through the reactor volume:

$$T|_{t=0} = T_0 \tag{26}$$

$$\alpha_i|_{t=0} = \alpha_{i0} \tag{27}$$

Here, the index 0 marks initial values of the temperature and conversion. The boundary conditions of the first, second, and third kind can be expounded:

1st kind: $T|_{wall} = T_e(t)$ Temperature $\tag{28}$

2nd kind: $q|_{wall} = q(t)$ Heat flow $\tag{29}$

3rd kind: $-\lambda \frac{\partial T}{\partial n}|_s = \chi(T_{wall} - T_e)$ $\tag{30}$

Newton's law of heat exchange

where the indices "wall" and "e" relate to the parameters on the boundary and the environment, respectively [29].

The SADT, CT, ET, and T_{cr} values for 25-kg package and 400-kg reactor from energy hazard simulation are exhibited in Table 9. The decomposition reaction energy stability of package was observed greater than that of reactor. The stability and applicability are better as the reactor size decreases. The results of energy hazard simulation also proved that the smaller size container has a greater exothermal extent for containment of OPs than larger one. Therefore, an accurate procedure to determine the thermokinetic parameters and the runaway hazard was developed for BPO, DCPO, and LPO that could be applied toward energy reduction and inherently safer designs (ISDs) for application, shipping, and storage of these substances.

Conclusions and outlook

From a series of examinations, the thermal runaway reactions of BPO, DCPO, and LPO were studied using non-isothermal and simulation via DSC technique and TSS program. Modeling simulation was fully exploited to display the thermokinetic parameters and energy safety parameters precisely to provide the energy hazard information for transportation or storage. We conducted an effective analysis procedure and modeled for the energy-

induced hazard parameters of three solid OPs of BPO, DCPO, and LPO with the simulation method. Future studies will focus on the reaction pathways of the solid OPs analysis in various batch reactors and packages under different perceived scenarios.

References

1. Dou Z, Jiang JC, Wang ZR, Zhao SP, Yang HQ, Mao GB. Kinetic analysis for spontaneous combustion of sulfurized rust in oil tanks. J Loss Prev Process Ind. 2014;32:387–92.
2. Dou Z, Jiang JC, Zhao SP, Zhang WX, Ni L, Zhang MG, Wang ZR. Analysis on oxidation process of sulfurized rust in oil tank. J Therm Anal Calorim. 2017;128:125–34.
3. Liu SH, Shu CM, Hou HY. Applications of thermal hazard analyses on process safety assessments. J Loss Prev Process Ind. 2015;33:59–69.
4. Duh YS. Chemical kinetics on thermal decompositions of cumene hydroperoxide in cumene studied by calorimetry: an overview. Thermochim Acta. 2016;637:102–9.
5. Liu SH, Hou HY, Chen JW, Weng SY, Lin YC, Shu CM. Effects of thermal runaway hazard for three organic peroxides conducted by acids and alkalines with DSC, VSP2, and TAM III. Thermochim Acta. 2013;566:226–32.
6. Lv JY, Chen WH, Chen LP, Tian YT, Yan JJ. Thermal risk evaluation on decomposition processes for four organic peroxides. Thermochim Acta. 2014;589:11–8.
7. Lizarraga E, Zabaleta C, Palop JA. Thermal behavior of quinoxaline 1,4-di-N-oxide derivatives. J Therm Anal Calorim. 2017;127:1655–61.
8. Chen WC, Shu CM. Prediction of thermal hazard for TBPTMH mixed with BPO through DSC and isoconversional kinetics analysis. J Therm Anal Calorim. 2016;126:1937–45.
9. Yamamoto YK, Miyake A. Influence of a mixed solvent containing ionic liquids on the thermal hazard of the cellulose dissolution process. J Therm Anal Calorim. 2017;127:743–8.
10. Zhang GY, Jin SH, Li LJ, Li YK, Wang DQ, Li W, Zhang T, Shu QH. Thermal hazard assessment of 4,10-dinitro-2,6,8,12-tetraoxa-4,10-diazaisowutrzitane (TEX) by accelerating rate calorimeter (ARC). J Therm Anal Calorim. 2016;126:467–71.
11. Tseng JM, Lin CP, Hung ST, Hsu J. Kinetic and safety parameters analysis for 1,1,-di-(tert-butylperoxy)-3,3,5-trimethylcyclohexane in isothermal and non-isothermal conditions. J Hazard Mater. 2011;192:1427–36.
12. Ho TC, Duh YS, Chen JR. Case studies of incidents in runaway reactions and emergency relief. Process Saf Prog. 1998;17:259–62.
13. Li XR, Koseki H, Iwata Y, Mok YS. Decomposition of methyl ethyl ketone peroxide and mixture with sulfuric acid. J Loss Prev Process Ind. 2004;17:23–8.
14. Liu SH, Hou HY, Shu CM. Thermal hazard evaluation of autocatalytic reaction for benzoyl peroxide by DSC and TAM III. Thermochim Acta. 2015;605:68–76.
15. Luo KM, Chang JG, Lin SH, Chang CT, Yeh TF, Hu KH, Kao CS. The criterion of critical runaway and stable temperatures in cumene hydroperoxide reaction. J Loss Prev Process Ind. 2001;14:229–39.
16. Ozawa T. A new method of analyzing thermogravimetric data. Bull Chem Soc. 1965;38:1881–6.
17. Flynn JH, Wall LA. J Res Natl Bur Stand Phys Chem. 1966;70:487–92.
18. Flynn JH, Wall LA. A quick, direct method for the determination of activation energy from thermogravimetric data. J Polym Sci. 1966;4:323–8.
19. Lin CP, Tseng JM. Green technology for improving process manufacturing design and storage management of organic peroxide. Chem Eng J. 2012;180:284–92.
20. Chen JR, Cheng SY, Yuan MH, Kossoy AA, Shu CM. Hierarchical kinetic simulation for autocatalytic decomposition of cumene hydroperoxide at low temperatures. J Therm Anal Calorim. 2009;96:751–8.
21. You ML, Liu MY, Wu SH, Chi JH, Shu CM. Thermal explosion and runaway reaction simulation of lauroyl peroxide by DSC tests. J Therm Anal Calorim. 2009;96:777–82.
22. Lin CP, Tseng JM, Chang YM, Liu SH, Shu CM. Modeling liquid thermal explosion reactor containing tert-butyl peroxybenzoate. J Therm Anal Calorim. 2010;102:587–95.
23. Lin CP, Chang CP, Chou YC, Chu YC, Shu CM. Modeling solid thermal explosion containment on reactor HNIW and HMX. J Hazard Mater. 2010;176:549–58.
24. Kossoy AA, Shienman IY. Comparative analysis of the method for SADT determination. J Hazard Mater. 2007;143:626–38.
25. Hou HY, Shu CM, Duh YS. Exothermic decomposition of cumene hydroperoxide at low temperature conditions. AIChE J. 2001;47:1893–6.
26. STARe Software with Solaris Operating System. Operating instructions. Stockholm: Mettler Toledo; 2017.
27. You ML, Tseng JM, Liu MY, Shu CM. Runaway reaction of lauroyl peroxide with nitric acid by DSC. J Therm Anal Calorim. 2010;102:535–9.
28. Liu SH, Lin CP, Shu CM. Thermokinetic parameters and thermal hazard evaluation for three organic peroxides by DSC and TAM III. J Therm Anal Calorim. 2011;106:165–72.
29. Thermal safety software (TSS). St Petersburg Russia: ChemInform Saint-Petersburg (CISP) Ltd. 2016. http://www.cisp.spb.ru.
30. Kossoy AA, Benin AI, Akhmetshin YG. An advanced approach to reactivity rating. J Hazard Mater. 2005;118:9–17.
31. Kossoy AA, Akhmetshin YG. Identification of kinetic models for the assessment of reaction hazards. Process Saf Prog. 2007;26:209–20.
32. Kossoy AA, Hofelich T. Methodology and software for reactivity rating. Process Saf Prog. 2003;22:235–40.
33. Lu KT, Chen TC, Hu KH. Investigation of the decomposition reaction and dust explosion characteristics of crystalline benzoyl peroxides. J Hazard Mater. 2009;161:246–56.
34. Zaman F, Beezer AE, Mitchell JC, Clarkson Q, Elliot J, Davis AF, Willson RJ. The stability of benzoyl peroxide by isothermal microcalorimetry. Int J Pharm. 2001;277:133–7.
35. Lu KT, Chen TC, Hu KH. Investigation of the decomposition reaction and dust explosion characteristics of crystalline dicumyl peroxide. Process Saf Environ Prot. 2010;88:356–65.
36. Wu SH, Shyu ML, I YP, Chi JH, Shu CM. Evaluation of runaway reaction for dicumyl peroxide in a batch reactor by DSC and VSP2. J Loss Prev Process Ind. 2009;22:721–7.
37. Duh YS, Wu XH, Kao CS. Hazard ratings for organic peroxides. Process Saf Prog. 2008;27:89–99.
38. Frank-Kamenetskii DA. Diffusion and heat exchange in chemical kinetics. Princeton: Princeton University; 1955.
39. Frank-Kamenetskii DA. Diffusion and heat exchange in chemical kinetics. 2nd ed. New York, USA: Plenum Press; 1969.
40. Material safety data sheet (2007) Akzo Nobel Polymer Chemicals Bv. P.O. Box 247, 3800 AE Amersfoort, Netherlands
41. Recommendations on the transport of dangerous goods, manual of tests and criteria, 4th rev edn. New York, USA (2003)